LETTER

Giant osmotic energy conversion measured in a single transmembrane boron nitride nanotube

Alessandro Siria[1], Philippe Poncharal[1], Anne-Laure Biance[1], Rémy Fulcrand[1], Xavier Blase[2], Stephen T. Purcell[1] & Lydéric Bocquet[1]

New models of fluid transport are expected to emerge from the confinement of liquids at the nanoscale[1,2], with potential applications in ultrafiltration, desalination and energy conversion[3]. Nevertheless, advancing our fundamental understanding of fluid transport on the smallest scales requires mass and ion dynamics to be ultimately characterized across an individual channel to avoid averaging over many pores. A major challenge for nanofluidics thus lies in building distinct and well-controlled nanochannels, amenable to the systematic exploration of their properties. Here we describe the fabrication and use of a hierarchical nanofluidic device made of a boron nitride nanotube that pierces an ultrathin membrane and connects two fluid reservoirs. Such a transmembrane geometry allows the detailed study of fluidic transport through a single nanotube under diverse forces, including electric fields, pressure drops and chemical gradients. Using this device, we discover very large, osmotically induced electric currents generated by salinity gradients, exceeding by two orders of magnitude their pressure-driven counterpart. We show that this result originates in the anomalously high surface charge carried by the nanotube's internal surface in water at large pH, which we independently quantify in conductance measurements. The nano-assembly route using nanostructures as building blocks opens the way to studying fluid, ionic and molecule transport on the nanoscale, and may lead to biomimetic functionalities. Our results furthermore suggest that boron nitride nanotubes could be used as membranes for osmotic power harvesting under salinity gradients.

The field of nanofluidics has developed recently as a result of the characteristic length scale in fluidic systems being reduced to the nanometre range. From a fundamental point of view, novel transport properties are expected to emerge from the combination of strong confinement and the importance of surface properties on the nanoscale[4], and such properties may lead to technological breakthroughs. Accordingly, studying the physical and chemical interactions of water and ions with the confining structure is crucial to discovering new fluidic properties, as exemplified by the design of fluidic diodes[5,6] and nanofluidic transistors[7]. Fast mass and ion transport through carbon nanotubes was recently demonstrated[8–11], suggesting that water flow in such carbon-based pipes is nearly frictionless[12–14]. Several recent molecular simulations have suggested that boron nitride nanotubes (BNNTs), which have the crystallographic structure of carbon nanotubes but have radically different electronic properties[15], show great potential for water and ion transport[16,17]. However, unlike for carbon nanotubes, nanofluidic transport in BNNTs has not yet been studied experimentally.

In this work, we report the fabrication of a new class of nanofluidic devices and study the fluid transport properties inside a single BNNT. The results may have application in renewable-energy harvesting. Our hierarchical nanofluidic device is made of a single BNNT connecting two reservoirs across an impermeable, solid-state membrane (Fig. 1). This transmembrane nanotube (t-BNNT) configuration combines the advantages of an ideal cylindrical nanopipe geometry with the versatility of solid-state nanopore devices[18,19]. It allows fluid transport in the nanopipe to be probed under electric, pressure and chemical forcings, and their combinations. The t-BNNT consists of a single BNNT inserted into a hole in a silicon nitride (SiN) membrane. A single hole with a diameter of between 100 and 200 nm is drilled through the membrane using a FIB. An individual multiwalled BNNT is glued at the extremity of an electrochemically etched tungsten tip and its apex is opened using electric field ion evaporation (Supplementary Methods). The insertion of the nanotube into the hole is realized *in situ* in an SEM by nanomanipulation (Fig. 1a and Supplementary Methods). The movements of the tip are controlled by a home-made nanomanipulator consisting of five-axis piezo-inertial motors, which allows us to insert the nanotube into the membrane with nanometre precision. Once the tube is in place, the hole is sealed with cracked naphthalene using local electron-beam-induced deposition. The tip is then retracted, producing a telescopic sliding of the internal walls of the nanotube (Fig. 1a). This step ensures that the inner surface of the nanotube is atomically flat and that both extremities are fully open, thus avoiding inner defects in the channel. A final inspection using TEM allows the quality and inner diameter of the nanotubes to be checked and measured. We studied tubes with inner radii of $R \approx 15$–40 nm and lengths of $L \approx 1\,\mu m$.

The membrane traversed by the BNNT is then squeezed between two macroscopic fluid reservoirs containing potassium chloride (KCl) solutions of various concentrations, with controlled pH (Fig. 1b). We use Ag/AgCl electrodes to measure the electric current passing through the t-BNNT, with a precision in the picoampere range. In addition to the direct TEM visualization of the system, which allows us to verify the integrity of the transmembrane nanotube both before and after fluidic experimentation, benchmark measurements and experimental cross-checks are systematically performed to ensure that transport occurs exclusively through the BNNT (Supplementary Methods).

Our final interest in this work concerns electrical transport induced by salinity gradients in individual BNNTs, which is known as diffusio-osmosis[20,21]. However, we start by first characterizing the response of the BNNT to voltage and pressure drops, which provide key information on the BNNT's surface properties. Accordingly, the ion current, I, generated through the t-BNNT under an electric potential drop, ΔV, is first measured as a function of salt concentration (Fig. 2a). The electric conductance, $G = I/\Delta V$, and corresponding conductivity, K, defined as $K = GL/\pi R^2$, are deduced as functions of salt concentration (Fig. 2b). For a given tube, these conductance and conductivity curves show saturation of the conductance for low salt concentration. This observation is a signature of a charged confining surface[22], which is in strong contrast with the behaviour reported for carbon nanotubes[11]. The predicted conductance is[4]

$$G = 2e^2\mu C_s \frac{\pi R^2}{L} + e\mu \frac{2\pi R}{L}|\Sigma|(1+\alpha) \qquad (1)$$

where C_s is the KCl concentration, e is the electronic charge, $\mu = (\mu_K + \mu_{Cl^-})/2 = 4.8 \times 10^{11}\,\mathrm{s\,kg^{-1}}$ is the KCl mobility and Σ is the surface charge density on the BNNT surface (in $\mathrm{C\,m^{-2}}$). The correction $\alpha = (2\pi\lambda_B\mu\eta)^{-1} \approx 1$ accounts for the electro-osmotic

[1]Institut Lumière Matière, UMR5306 University Lyon 1-CNRS, 69622 Villeurbanne, France. [2]Institut Néel, UPR CNRS 2940 and Université Joseph Fourier, 38042 Grenoble, France.
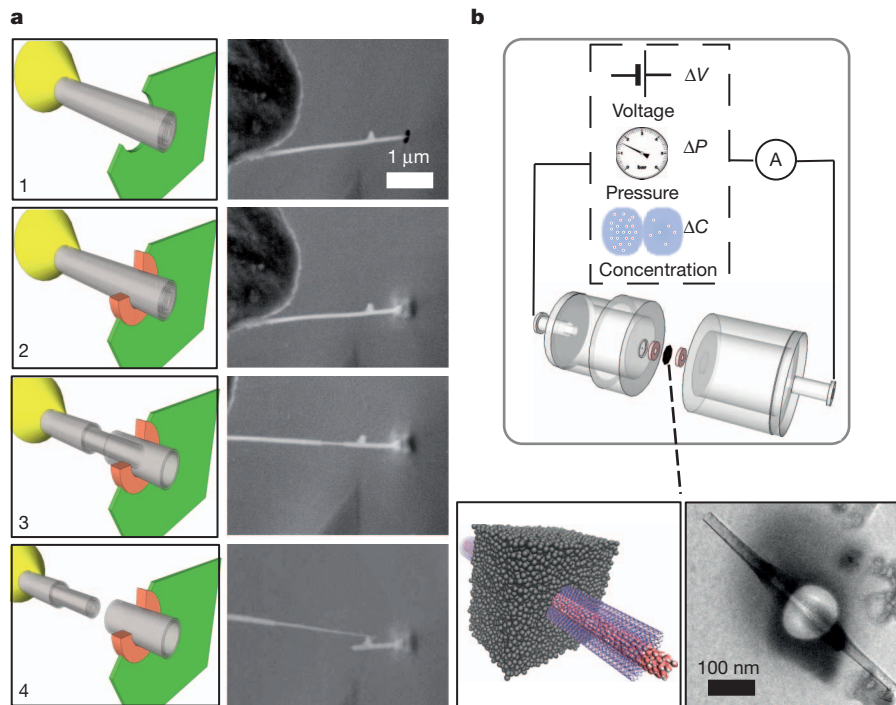
Figure 1 | Hierarchical single nanotube nanofluidic set-up. a, *In situ* nanomanipulation of a BNNT (left, sketch; right, scanning electron microscope (SEM) images): 1, insertion of a BNNT (grey) through a nanopore drilled in a SiN membrane (green) using a focused ion beam (FIB); 2, carbon sealing of the FIB-drilled hole using local electron-beam-induced deposition (orange); 3, telescopic retraction of internal walls of the BNNT; 4, finalized transmembrane BNNT device. **b**, Top, schematic of the experimental set-up for measuring fluid transport through the single BNNT. Bottom, sketch of the final transmembrane BNNT for nanofluidic measurements (left) and its experimental realization, imaged by transmission electron microscopy (TEM) (right).

contribution to the conductance ($\lambda_B = 0.7$ nm is the Bjerrum length and η is the water viscosity). At low pH (pH 5 in Fig. 2a, b), the calculated surface charge is found to increase slightly as the diameter of the tube is decreased, with a typical value of $\Sigma \approx 0.1$ C m^{-2} (Fig. 2b). Although this surface charge is already very large, we measure a large—and reversible—increase with pH, with Σ rising to 1 C m^{-2} for pH $\sim$11 (Fig. 2c), which corresponds to $9e$ nm^{-2} on the BNNT surface. This exceeds typical surface charge densities by at least an order of magnitude[23]. Although zeta potential measurements on BN powders have consistently suggested that the BN surface is charged and that the charge is dependent on pH[24], the observed chemical reactivity of the BN surface as a function of pH has not been documented up to now. Our results are consistent with a possible chemical equilibrium, $BN_3 + H_2O \rightleftharpoons BN_3 - OH^- + H^+$, in analogy with the reactivity of boric acid, with a corresponding reaction constant K_a.

This unexpected chemical reactivity is supported by preliminary *ab initio* simulations, which demonstrate that an 'activated' boron site, that is, one with a hydrogen atom bound to a nitrogen atom, can indeed seed water dissociation on a BN sheet (Supplementary Methods). It is well documented[25] that defects in the large bandgap of the ionic h-BN system (the planar hexagonal BN sheet) lead to open-shell in-gap states prone to capturing charge. This behaviour echoes that recently described at the non-polar GaN surface, which was shown to generate surface-bound OH$^-$ fragments through spontaneous water dissociation[26]. In the present situation, a charge regulation model[23] accordingly reproduces the pH dependence of the charge (Fig. 2c), providing a value of p$K_a \approx 5.5$ for the equilibrium constant (with the density of chargeable sites identified as the surface density of boron in the BNNT, $\Gamma = 18$ nm^{-2}; see Supplementary Methods). This value is also consistent with the pK_a of porous glass, with an expected surface excess of boron[27].

The response of the confined fluid to a pressure drop across the t-BNNT furnishes an alternative, sensitive probe to assess the coupled fluid–ion dynamics. By transporting ions in the electric double layer,
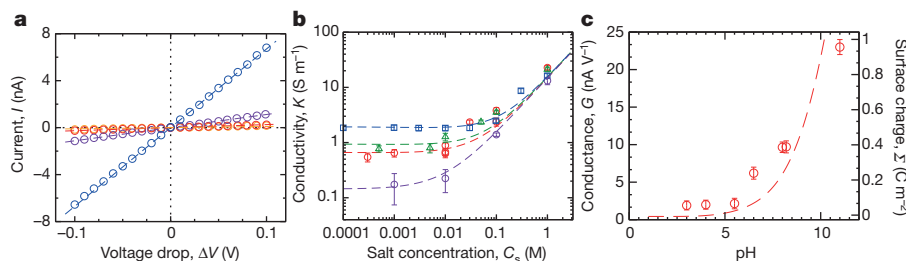

Figure 2 | Electrical conductance and chemical reactivity of the BNNT. a, Ion current versus voltage drop for $C_s = 1$ M (blue), 10^{-1} M (purple), 10^{-2} M (orange) and 10^{-3} M (red) at pH 5, for a t-BNNT with $\{R, L\} = \{29$ nm, 900 nm$\}$. Dashed lines are linear fits, from which conductance, $G = I/\Delta V$, and conductivity, $K = GL/\pi R^2$, are determined. **b**, Conductivity versus salt concentration for various t-BNNTs, with $\{R, L\} = \{40$ nm, 1,250 nm$\}$ (purple), $\{29$ nm, 900 nm$\}$ (red), $\{22$ nm, 1,500 nm$\}$ (green) and $\{15$ nm, 800 nm$\}$ (blue), at pH 5. Dashed lines are predictions using equation (1) with $\Sigma = 25, 85, 90, 125$ mC m^{-2}. **c**, Dependence on pH of the conductance and the surface charge, deduced from equation (1), for a t-BNNT with $\{R, L\} = \{29$ nm, 900 nm$\}$ and $C_s = 10^{-2}$ M. Error bars, 1 s.d.
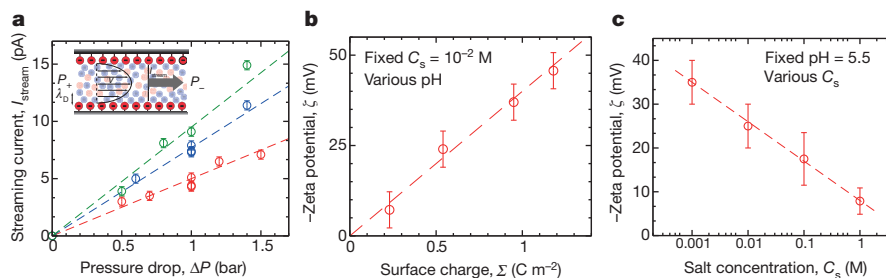
Figure 3 | Pressure-driven streaming. **a**, Streaming current induced by a pressure drop, for a t-BNNT with $\{R, L\} = \{29\text{ nm}, 900\text{ nm}\}$, pH 7 (red), 8.5 (blue) and 10 (green), and $C_s = 10^{-2}$ M. The straight lines are the corresponding linear fits. Inset, sketch of the pressure-driven streaming current. $\Delta P = P_+ - P_-$, pressure drop. **b**, Calculated zeta potential versus surface charge for $C_s = 10^{-2}$ M and pH 5–11.5. The measured surface charge is determined from equation (1) for each pH. The dashed line is a linear fit. **c**, Measured zeta potential versus salt concentration for a t-BNNT with $\{R, L\} = \{40\text{ nm}, 1{,}250\text{ nm}\}$ and pH 5.5. The dashed line is a linear fit of ζ versus $\log(C_s)$. Error bars, 1 s.d.

an electric streaming current, I_{stream}, typically of a few picoamperes, results from the pressure-driven flow (Fig. 3). This provides a measurement of the electro-osmotic mobility and corresponding zeta potential, ζ, here defined by the Smoluchowski relationship[23], $I_{stream} = -(\varepsilon \zeta/\eta) A(\Delta P/L)$, where ε is the dielectric permittivity of water, $A = \pi R^2$ is the tube cross-sectional area and ΔP is the applied pressure drop. A pressure drop of up to 1.5 bar is applied between the two fluid reservoirs by means of a voltage-controlled valve (Fig. 1b), and the resulting electric current, $I_{stream}(\Delta P)$, is measured (Fig. 3a). Like the surface charge, Σ, the corresponding zeta potential is found to increase with pH; in Fig. 3b it is shown to be nearly linearly proportional to $\Sigma(\mathrm{pH})$ as obtained from the independently measured surface conductance. It is also a slowly decreasing function of the salt concentration, varying linearly with $pC_s = -\log_{10}(C_s)$ (Fig. 3c). Overall, the value of the zeta potential is markedly smaller than the estimated surface potential, as calculated from, for example, the non-linear Poisson–Boltzmann equation (Supplementary Methods). Such behaviour has been reported for other types of charged interface and its origin is the subject of active investigations[28].

Together, these first measurements highlight the presence of a very large, pH-sensitive surface charge carried by the inner walls of BNNTs. To our knowledge, values of Σ as high as 1 C m^{-2} have not been reported up to now. We now demonstrate that this property has a key impact on the osmotic transport through the nanotube, whereby an electric current is generated by a difference in salt concentration. This phenomenon is particularly interesting in the context of energy conversion from the mixing of masses of water with different salinities. However, although as much as 0.7 kW h of energy could theoretically be captured per cubic metre of water[3], boosting the efficiency of the energy extraction process remains a key challenge.

We use different KCl concentrations, $C_{s,I}$ and $C_{s,II}$, in the range 10^{-3}–1 M in the two reservoirs and measure the resulting electric current for a variety of concentration ratios, $C_{s,I}/C_{s,II}$. The bare current is corrected for the contribution resulting from the Nernst potential originating in the difference in salt concentration at the two electrodes[29] (Supplementary Methods). As shown in Fig. 4a, a very large, osmotically driven current is measured. It is in the nanoampere range, whereas the pressure-driven streaming current is in the picoampere range (Fig. 3). Furthermore, we find that it increases linearly with the logarithm of the salinity ratio, $\Delta\log(C_s) = \log(C_{s,I}/C_{s,II})$:

$$I_{osm} = K_{osm}\Delta\log(C_s) \qquad (2)$$

Here $K_{osm} \approx 0.07$–0.16 nA is the transport coefficient for the nanotube in Fig. 4, with pH ranging from 5.5 to 11, and is almost linearly proportional to the surface charge, Σ (Fig. 4a, inset).

The nanotube is not ion-selective for the configuration presented in Fig. 4a, because no Debye layer overlap occurs here. The origin of the produced current therefore differs from the ion-selective mechanism usually assumed in the osmotic generation of energy, known as reversed electrodialysis, which uses ion exchange membranes to convert a salinity gradient into electric energy[3,29]. Rather, we suggest that this osmotic current results from the diffusio-osmotic flux induced by the difference in salt concentration at the inner interface of the tube[20]. Although no global osmotic pressure drop builds up in this permeable configuration, the salt concentration difference builds an osmotic pressure gradient within the diffuse layer at the interfaces[20,21] (Fig. 4c). Accordingly, the diffusio-osmotic flow, expressed in terms of the diffusio-osmotic velocity, V_{DO}, results from a balance between viscous flow and the osmotic pressure gradient within the Debye layer: $\eta V_{DO}/\lambda_D \propto \lambda_D k_B T \nabla C_s$. Here $\nabla C_s = \Delta C_s/L$ is the salt concentration gradient, $\lambda_D = (8\pi\lambda_B C_s)^{-1/2}$ is the Debye length, T is the temperature and k_B is the Boltzmann constant. The diffusio-osmotic velocity can then be written as $V_{DO} = \mu_{DO}\nabla\log(C_s)$, where $\nabla\log(C_s) =$
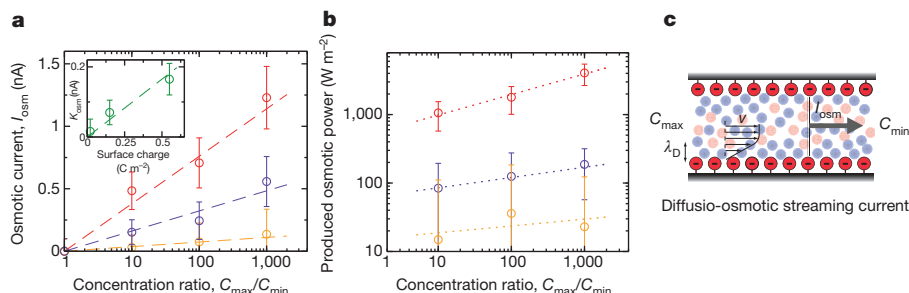

Figure 4 | Osmotic power generation under salinity gradients. **a**, Osmotic streaming current versus concentration difference for a t-BNNT with $\{R, L\} = \{40\text{ nm}, 1{,}250\text{ nm}\}$ and pH 5.5 (yellow), 9.5 (purple) and 11 (red). The experimental points show measurements for various salt concentrations in the two reservoirs, with C_{min} and C_{max} in the range 10^{-3}–1 M. Error bars follow from the corresponding error analysis. Dashed lines are linear fits: $I_{osm} = K_{osm}\log(C_{max}/C_{min})$. Inset, osmotic mobility versus surface charge. Surface charge is obtained from independent conductance measurements. The dashed line is a linear fit: $K_{osm} \approx 0.33\Sigma$. **b**, Corresponding power density (per unit surface of the BNNT) for the three values of pH. Dotted lines are a guide to the eye. In the present graph, the minimum concentration is fixed to $C_{min} = 10^{-3}$ M. **c**, Sketch of the osmotically driven streaming current under a salt concentration difference, $C_{max} - C_{min}$.

$\Delta \log(C_s)/L$ and the diffusio-osmotic mobility scales as $\mu_{DO} \propto k_B T/\eta \lambda_B \approx 10^{-9} \, m^2 \, s^{-1}$ (ref. 20). This diffusio-osmotic flow drags the charges in the double layer at the BNNT interface (Fig. 4c). The predicted osmotic current is written accordingly as $I_{osm} \propto 2\pi R \Sigma V_{DO}$:

$$I_{osm} \approx \frac{2\pi R \Sigma}{L} \frac{k_B T}{\eta \lambda_B} \Delta \log(C_s) \quad (3)$$

A rigorous derivation of the osmotic current is given in Supplementary Methods and confirms the scaling described by equation (3). This expression captures the observed functional dependence of the osmotic current on the salinity ratio (Fig. 4a), with a predicted transport mobility (here expressed in nA) proportional to Σ for large surface charge, $K_{osm}^{theo} \approx 0.2\Sigma$, in good quantitative agreement with experiments (Fig. 4a, inset).

Furthermore, the complete theoretical model predicts that for small Σ values the osmotic mobility, K_{osm}, decreases to zero like Σ^3 (Supplementary Methods): this points to the unique qualitiy of BN as a confining material, whose giant surface charge generates much larger osmotic current than for alternative materials. Also, the measured osmotic current is larger than the pressure-driven streaming currents plotted in Fig. 3a. This is due to a combination of factors. First, owing to the difference in microscopic origin of the two phenomena, the osmotic mobility is much more sensitive to large surface charges than its electro-osmotic counterpart (Supplementary Methods). Second, the osmotic pressure drop that exists inside the double layer for the osmotically driven phenomenon is much larger than the external pressure drop that can usually be applied. Typically, $\Delta P_{osm} \approx 50$ bar inside the double layer for $\Delta C_s = 1$ M as compared with the applicable pressure range for pressure-driven flows, ΔP_{ext}, which is at most a few bars. Under such large pressures, a streaming current of up to 0.5 nA could be extrapolated, although the origins of the two phenomena are clearly different. Finally, the predicted linear scaling of I_{osm} as a function of nanotube radius makes the osmotic generation more efficient for smaller tubes than its pressure-driven counterpart, which is proportional to the square of tube radius (Supplementary Methods).

The t-BNNT device thus generates electrical energy from a salinity gradient. The maximum power generated is $P_{max} = I_{osm}^2/4G_{ion} = K_{osm}^2/4G_{ion}[\Delta \log(C_s)]^2$ (ref. 29), which leads to a power density per unit tube surface of $\mathcal{P}_{max} = P_{max}/\pi R^2$, reaching $4 \, kW \, m^{-2}$ for the single BNNT (Fig. 4b). This single-nanotube result could be extrapolated to a macroscopic BN membrane[30], with a similar BNNT density of $\sim 10^{10} \, cm^{-2}$, for which the predicted power density reaches values in the same range ($kW \, m^{-2}$). These values exceed by several orders of magnitude the reported power densities, usually of a few tens of watts per square metre, using classical reversed electrodialysis with alternative exchange membranes[3]. Our results thus demonstrate the impressive performance of BNNT membranes for energy conversion from the mixing of water masses with different salinities, making them potentially superior to photovoltaics. They open a new avenue in the exploration of new sources of renewable 'blue energy'.

METHODS SUMMARY

The transmembrane nanotube device is realized by *in situ* SEM insertion of a nanotube in a FIB-drilled SiN membrane. The nanotube is opened via *in situ* TEM field evaporation of the apex. The membrane and nanotube are positioned on a five-axis nanomanipulator allowing x–y–z translation (Attocube ANPx-z51) along with θ–ϕ rotation (Attocube ANR51). A first, coarse, approach is performed with 100-nm stick-and-slip steps of the inertial motors. The final insertion of the nanotube in the membrane is done with nanometre precision, by applying a d.c. voltage to the piezoelectric element of the motors. Once inserted, an electron beam is focused on the hole and a gas injection system is used to inject naphthalene (C_8H_8) locally, which is decomposed under electron-beam irradiation and subsequently fills the hole with a water-impermeable and electrically insulating material. The transmembrane nanotube is then squeezed between two reservoirs, allowing for measurements of the ion current induced by voltage drop, pressure drop and salt concentration difference.

1. Sparreboom, W., van den Berg, A. & Eijkel, J. C. T. Principles and applications of nanofluidic transport. *Nature Nanotechnol.* **4**, 713–720 (2009).
2. Rasaiah, J. C., Garde, S. & Hummer, G. Water in non polar confinement: from nanotubes to proteins and beyond. *Annu. Rev. Phys. Chem.* **59**, 713–740 (2008).
3. Logan, B. E. & Elimelech, M. Membrane-based processes for sustainable power generation using water. *Nature* **488**, 313–319 (2012).
4. Bocquet, L. & Charlaix, E. Nanofluidics, from bulk to interfaces. *Chem. Soc. Rev.* **39**, 1073–1095 (2010).
5. Karnik, R., Duan, C., Castelino, K., Daiguji, H. & Majumdar, A. Rectification of ionic current in a nanofluidic diode. *Nano Lett.* **7**, 547–551 (2007).
6. Siwy, Z. & Fulinski, A. Fabrication of a synthetic nanopore ion pump. *Phys. Rev. Lett.* **89**, 198103 (2002).
7. Schasfoort, R. B. M., Schlautmann, S., Hendrikse, J. & van den Berg, A. Field-effect flow control for microfabricated fluidic networks. *Science* **286**, 942–945 (1999).
8. Majumder, M., Chopra, N., Andrews, R. & Hinds, B. J. Enhanced flow in carbon nanotubes. *Nature* **438**, 44 (2005).
9. Holt, J. K. *et al.* Fast mass transport through sub-2-nanometer carbon nanotubes. *Science* **312**, 1034–1037 (2006).
10. Whitby, M., Cagnon, L., Thanou, M., &. Quirke, N. Enhanced fluid flow through nanoscale carbon pipes. *Nano Lett.* **8**, 2632–2637 (2008).
11. Liu, H. *et al.* Translocation of single stranded DNA through single-walled carbon nanotubes. *Science* **327**, 64–67 (2010).
12. Hummer, G., Rasaiah, J. C. & Noworyta, J. P. Water conduction through the hydrophobic channel of a carbon nanotube. *Nature* **414**, 188–190 (2001).
13. Falk, K., Sedlmeier, F., Joly, L., Netz, R. R., &. Bocquet, L. Molecular origin of fast water transport in carbon nanotube membranes: superlubricity versus curvature dependent friction. *Nano Lett.* **10**, 4067–4073 (2010).
14. Joseph, S. & Aluru, N. R. Why are carbon nanotubes fast transporters of water? *Nano Lett.* **8**, 452–458 (2008).
15. Arenal, R., Blase, X. & Loiseau, A. Boron-nitride and boron-carbonitride nanotubes: synthesis, characterization and theory. *Adv. Phys.* **59**, 101–179 (2010).
16. Won, C. Y. & Aluru, N. R. Water permeation through a subnanometer boron nitride nanotube. *J. Am. Chem. Soc.* **129**, 2748–2749 (2007).
17. Hilder, T. A., Gordon, D., Chung, S.-H. & Salt rejection. and water transport through boron nitride nanotubes. *Small* **5**, 2183–2190 (2009).
18. Li, J. *et al.* Nanoscale ion beam sculpting. *Nature* **412**, 166–169 (2001).
19. Dekker, C. Solid state nanopores. *Nature Nanotechnol.* **2**, 209–215 (2007).
20. Anderson, J. L. Colloid transport by interfacial forces. *Annu. Rev. Fluid Mech.* **21**, 61–99 (1989).
21. Fair, J. C. & Osterle, J. F. Reverse electrodialysis in charged capillary membranes. *J. Chem. Phys.* **54**, 3307–3316 (1971).
22. Stein, D., Kruithof, M. & Dekker, C. Surface charge governed ion transport in nanofluidic channels. *Phys. Rev. Lett.* **93**, 035901 (2004).
23. Hunter, R. J. *Foundations of Colloid Science* (Oxford Univ. Press, 1991).
24. Crimp, M. J., Oppermann, D. A. & Krehbiel, K. Suspension properties of hexagonal BN powders: effect of pH and oxygen content. *J. Mater. Sci.* **34**, 2621–2625 (1999).
25. Schmidt, T. M., Baierle, R. J., Piquini, P. & Fazzio, A. Theoretical study of native defects in BN nanotubes. *Phys. Rev. B* **67**, 113407 (2003).
26. Wang, J., Pedroza, L. S., Poissier, A. & Fernandez-Serra, M. V. Water dissociation at the GaN surface: structure, dynamics and surface acidity. *J. Phys. Chem. C* **116**, 14382–14389 (2012).
27. Altug, I. & Hair, M. L. Cation exchange in porous glass. *J. Phys. Chem.* **71**, 4260–4263 (1967).
28. Bonthuis, D. & Netz, R. Unraveling the effects of dielectric and viscosity profiles on electro-osmotic mobility and electric surface conductivity. *Langmuir* **28**, 16049–16059 (2012).
29. Kim, D.-K., Duan, C., Chen, Y.-F. & Majumdar, A. Power generation from concentration gradient by reverse electrodialysis in ion-selective nanochannels. *Microfluid. Nanofluid.* **9**, 1215–1224 (2010).
30. Bechelany, M. *et al.* Synthesis of boron nitride nanotubes by a template-assisted polymer thermolysis process. *J. Phys. Chem. C* **111**, 13378–13384 (2007).

Author Contributions L.B. conceived the project. P.P. and S.T.P. designed the transmembrane nanotube system. A.S. and P.P. constructed the experimental device with contributions from R.F. and A.-L.B. A.S., A.-L.B. and L.B. designed the fluidic system (with input from P.P.), performed measurements and conducted the experimental analysis. X.B. performed the *ab initio* simulations. L.B. wrote the manuscript with input from all authors.

Author Information Reprints and permissions information is available at www.nature.com/reprints. The authors declare no competing financial interests. Readers are welcome to comment on the online version of the paper. Correspondence and requests for materials should be addressed to L.B. (lyderic.bocquet@univ-lyon1.fr).